Prediction Model of Cleavage Fracture Toughness of Ferrite Steel

Kazuki Shibanuma[1,*], Shuji Aihara[1], Motoyuki Matsubara[2], Hiroyuki Shirahata[3], Tsunehisa Handa[4]

[1] Department of Systems Innovation, The University of Tokyo, Tokyo 113-8656, Japan
[2] Hanshin Plant, Kubota Corporation, Hyogo 660-0857, Japan
[3] Oita R&D Lab., Nippon Steel & Sumitomo Metal Corporation, Oita 870-0992, Japan
[4] Joining & Strength Research Department, JFE Steel Corporation, Chiba 260-0835, Japan
* Corresponding author: shibanuma@fract.t.u-tokyo.ac.jp

Abstract A numerical model to quantitatively predict a cleavage fracture toughness in ferrite-cementite steel is proposed based on a microscopic fracture initiation process of three stages; (I) formation of fracture origin by cementite cracking, (II) propagation of the cementite crack into ferrite matrix, and (III) propagation across ferrite grain boundary. The fracture condition of Stage (I) is formulated as a ratio of cementite cracking based on experimental results of a tensile testing with notched specimens and SEM observation. Stage (II) and Stage (III) conditions are formulated based on a concept of fracture stress criterion. In the numerical model, an active zone is divided into finite volume elements. Ferrite grains and cementite particles are assigned based on their distributions into each volume element. Strain and stress at each volume element are calculated by a macroscopic FEA. Fracture is assumed to initiate at the time when the fracture conditions of the all stages are satisfied in any one of the volume elements. The model is validated by three point bend testing with notched specimens. The predicted values of fracture toughness show good agreement with the experimental results. Therefore, the effectiveness of the proposed model is found out.
Keywords Cleavage fracture, Fracture toughness, Multiscale, Fracture stress, Ferrite

1. Introduction

In order to prevent brittle fracture in steel structures, it is critically important to predict fracture toughness by clarification of crack initiation mechanism.

It is widely known that fracture appearance transition temperature of Charpy impact testing changes linearly with reciprocal of the square root of grain size [1]. The reason is, however, not clarified completely. It is also known that the fracture toughness depends on the size of brittle phase such as cementite [2]. In addition, several formulations to evaluate the influence of microstructures including the size of ferrite grain and brittle phase are proposed by Almond *et al*. [3], Petch [4] and Bingley [5]. However, there remains a problem to improve their accuracy.

The cleavage fracture of steel is generally interpreted by the weakest-link mechanism differently from the yielding and the work hardening. Scatter in the fracture toughness is therefore essential. This is a principal reason of the difficulty to quantify the influence of microstructures on fracture toughness. A formulation to evaluate the variation of fracture toughness was proposed by Beremin [6] based on the weakest-link theory. It was, however, based on the concept of the macroscopic continuum mechanics and thus was not able to clarify the relationship between the variation of the fracture toughness and microstructures.

In the present paper, a numerical model is proposed to quantitatively predict the influence of microstructures on the fracture toughness of ferrite-cementite steels, based on the formulation of the cleavage fracture initiation process.

2. Formulation of Cleavage Fracture Initiation Process

2.1. Process of fracture initiation

We assume that the process of cleavage fracture initiation in ferrite-cementite steels is composed of three stages; (I) formation of fracture origin by cementite cracking, (II) propagation of the crack in cementite into the ferrite matrix and formation of a cleavage crack, and (III) propagation of the cleavage crack across ferrite grain boundary. Schematic view of this process is shown in Fig. 1. It is assumed that a macroscopic brittle fracture occurs if fracture conditions of all the above stages are satisfied. In the following section, the fracture conditions of respective stages are formulated.

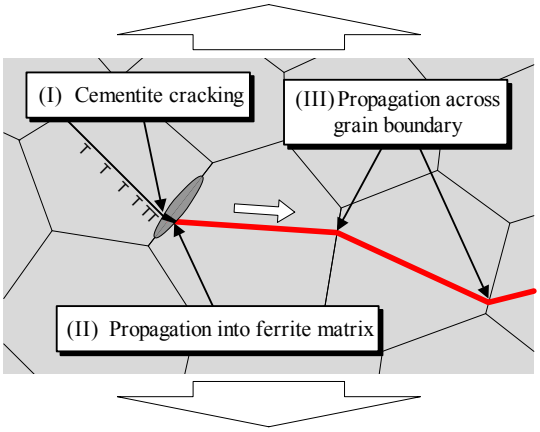

Fig. 1 Three stages of cleavage fracture initiation process

2.2. Formulations of fracture conditions

Stage (I). Formation of fracture origin by cementite cracking

We quantify the influencing factors on the cementite cracking based on experimental facts.

Test steels with various sizes of ferrite grains and cementite particles were produced and tensile testing with a circumferential notched round bar specimen was performed. The test steels were produced by laboratory scale vacuum melting and rolling. Two types of chemical compositions are employed, as shown in Table 1. It can be regarded that their compositions are practically the same except for carbon concentration. Seven types of steels were produced whose sizes of ferrite grains and cementite particles were systematically changed by combinations of controlled rolling, controlled cooling, normalizing and annealing processes. Definitions of symbols relating to the sizes of ferrite grains and cementite particles are shown in Table 2. Grain sizes of the steels were measured as area equivalent diameter by EBSD observation [7]. In addition, cementite particle thickness was measured as minor axis of approximated ellipse by FE-SEM observation of the microstructure etched by nital and an image analysis [8]. Representative values of ferrite grain size

Table 1 Chemical compositions of test steels [mass%]

Symbol	C	Si	Mn	P	S	Al	N
10	0.10	0.06	0.49	< 0.002	0.0005	0.010	0.0011
5	0.05	0.05	0.48	< 0.002	0.0003	0.010	0.0014

Table 2 Symbols of steels

Cementite size	**Ferrite grain size**		
	Large	Medium	Small
Large	10LL	-	5SL
Medium	10LM	10MM	-
Small	10LS	-	10SS / 5SS

Table 3 Representative values of grain size and cementite particle thickness and yield stress at room temperature

Symbol		10LL	10LM	10LS	10MM	10SS	5SL	5SS
Ferrite grain diameter [$\times 10^{-3}$ mm]	Average	57	63	58	38	16	27	23
	Max	218	226	229	104	47	67	45
Cementite thickness [$\times 10^{-3}$ mm]	99%max	0.83	0.41	0.24	0.43	0.20	0.66	0.20
	Max	1.87	1.02	0.66	1.21	0.49	1.15	0.44
Yield stress at room temperature [MPa]		161	170	171	215	247	213	248

and cementite particle thickness, together with yield stress at room temperature are shown in Table 3.

Quasi-static tensile test using circumferential notched round bar specimens was conducted. The specimen configuration is shown in Fig. 2. After tensile strain was applied, the specimen was unloaded and cementite cracking was observed. Extensometer gauge displacement at unloading was determined so that the maximum principal plastic strain at the minimum cross section is equal to 0.4. The displacement was estimated by a preliminary elasto–plastic FEA. An example of the numerical results is described as Fig. 3. The results show that the maximum principal plastic strain and stress change in the axial direction but are almost constant on each transverse cross section.

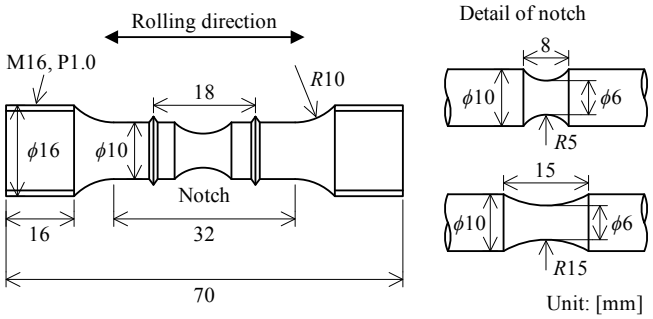

Fig. 2 Configuration of circumferential notched round bar specimen

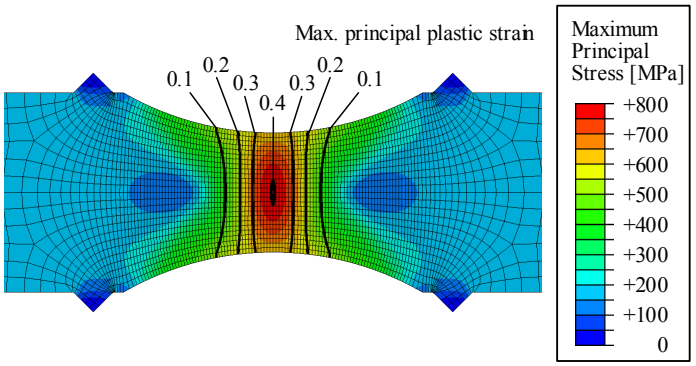

Fig. 3 Strain and stress distributions in circumferential notched round specimen (10MM, $R = 15$ mm, -80°C)

The unloaded specimen was cut in the axis direction. The maximum principal plastic strain and stress are assumed constant along the transverse direction on the cut surface. The cracked cementite was measured by scanning the surface in the transverse direction by SEM observation after polishing and etching. The applied strain can be varied by changing the scanning location in the axial direction.

The numbers of the cracked cementite particles were measured for the steels and conditions of temperature and strain. An example of the SEM images of the cracked cementite is shown in Fig. 4. Results of dependence of the number of the cracked cementite on the maximum principal plastic strain and the temperature for 10LM steel are shown in Fig. 5. The number of the cracked cementite is almost in proportion to the principal plastic strain. The results also show that the lower temperature makes the larger number of the cementite cracking.

The cementite cracking might be regarded as stress-controlled fracture. However, the stress applied to a cementite particle is controlled by the applied strain of the ferrite matrix. It can be understood that the larger deformation resistance of ferrite matrix makes the larger applied stress in the cementite particle. Furthermore, total number of the cementite particles must be proportional to carbon content if cementite size distribution remains unchanged.

Now, it may be rationalized that the number of cracked cementite particles is normalized by a parameter η, which is defined as a product of the applied maximum principal stress $\sigma_{\max}$ (normalized by Young's modulus E) and mass fraction of carbon r_C as

$$\eta = \frac{\sigma_{\max}}{E} r_C \tag{1}$$

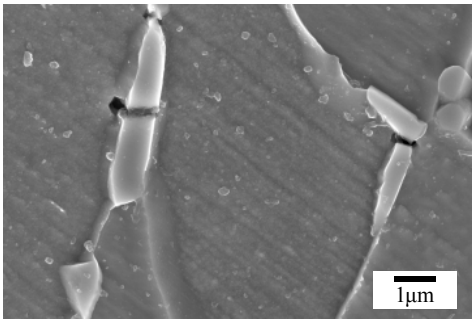

Fig. 4 SEM image of cracked cementite (10LM, $\varepsilon_p = 0.2$)

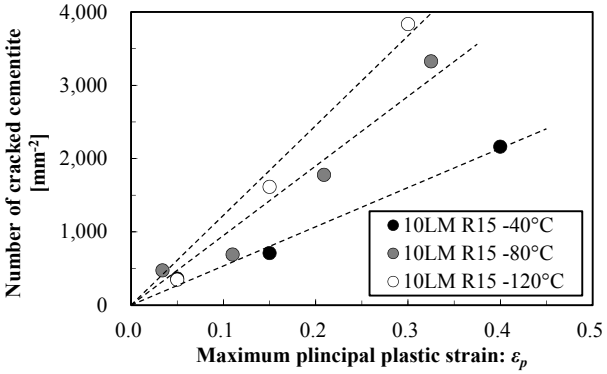

Fig. 5 Dependence of the number of cementite cracking on plastic strain and temperature

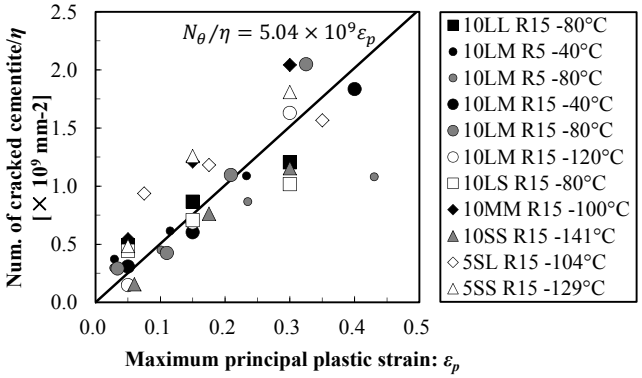

Fig. 6 Number of cracked cementite normalized by applied maximum principal stress and mass fraction of carbon

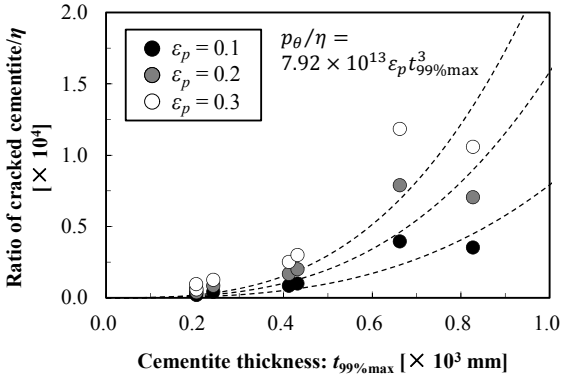

Fig. 7 Ratio of cementite cracking normalized by applied maximum principal stress and mass carbon content

Results of all the tests are shown in Fig. 6. Although a data scatter is found, the number of the cracked cementite particles mig ht be approximated as

$$\frac{N_\theta}{\eta} = 5.04 \times 10^9 \varepsilon_p \tag{2}$$

where N_θ is the number of the cracked cementite particles per unit area (1 mm^2) and ε_p is the maximum principal plastic strain. It is noted that N_θ/η is independent from the cementite particle thickness distribution.

A ratio of cementite cracking p_θ is defined as the number of the cracked cementite particles divided by the number of the all cementite particles per unit area. It is found that the ratio of the cementite cracking is higher in the steel with larger cementite size. Plots of p_θ/η related to $t_{99\%\max}$ (unit: mm) of each steel (see Table 3) are shown in Fig. 7. By fitting the relationship between p_θ/η and $t_{99\%\max}$, we obtain

$$\frac{p_\theta}{\eta} = 7.92 \times 10^{13} \varepsilon_p t_{99\%\max}^3 \tag{3}$$

as indicated by the lines in Fig. 7.

As a generalization of Eq. (3), the ratio of cementite cracking for arbitrary cementite particle thickness t (unit: mm) is expressed as

$$p_\theta = 7.92 \times 10^{13} \eta \varepsilon_p t^3 \quad (4)$$

Stage (II). Propagation of crack in cementite into ferrite matrix

Local fracture stress required for a propagation of a cementite crack into ferrite matrix was formulated by Petch [4]. We assume a fracture condition of Stage (II) as

$$\sigma_n \geq \sigma_{F\theta\alpha} \quad (5)$$

σ_n is a maximum normal stress on the {100}-plane of the ferrite grain because it is known that a cleavage fracture surface in a BCC polycrystal including ferrite-cementite steel are generally formed on a {100}-plane [9]. σ_n is calculated as

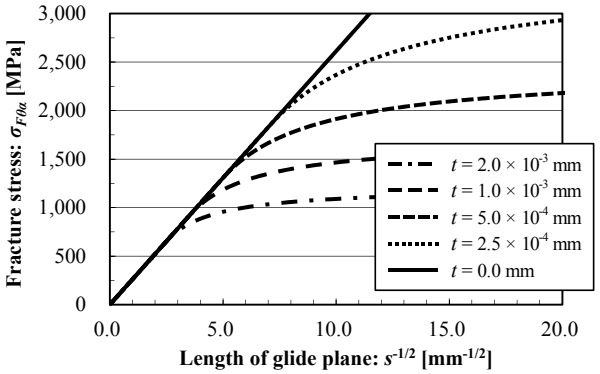

Fig. 8 Dependence of fracture stress $\sigma_{F\theta\alpha}$ on grain size d and cementite particle thickness t

$$\sigma_n = \max_{m=1,2,3} (\mathbf{n}_m)^T \cdot \boldsymbol{\sigma} \cdot \mathbf{n}_m \quad (6)$$

where $\mathbf{n}_m$ is a normal vector of the m-th {100}-plane and $\boldsymbol{\sigma}$ is a applied stress tensor.

$\sigma_{F\theta\alpha}$ in Eq (5) is the fracture stress of Stage (II) originally formulated by Petch [4] as

$$\sigma_{F\theta\alpha} = \begin{cases} \dfrac{4E\gamma_{\theta\alpha}}{\left(1+\dfrac{1}{\sqrt{2}}\right)(1-\nu^2)k_y\sqrt{s}} & (t_\theta < c_c) \\ \sqrt{\dfrac{4E\gamma_{\theta\alpha}}{\pi(1-\nu^2)t_\theta} - \dfrac{k_y^2 s}{8\pi^2 t_\theta^2}} - \dfrac{k_y\sqrt{s}}{2\sqrt{2}\pi t_\theta} & (t_\theta \geq c_c) \end{cases} \quad (7)$$

where ν is a Poisson's ratio. The definition of $\sigma_{F\theta\alpha}$ is slightly modified from the original one by replacing a ferrite grain diameter with a length of the dislocation line s. k_y is a locking parameter in the Hall-Petch law and is assumed to equal 20.7 MPa mm$^{1/2}$ based on our preliminary test. $\gamma_{\theta\alpha}$ is effective surface energy and is given as 10 J/m^2 [4]. c_c is critical cementite particle thickness defined as

$$c_c = \frac{\left(1+\dfrac{1}{\sqrt{2}}\right)(1-\nu^2)k_y^2 s}{8\pi E\gamma_{\theta\alpha}} \quad (8)$$

$\sigma_{F\theta\alpha}$ is derived from a comparison of the sum of energy release rate of the crack and piled-up dislocation energy with the effective surface energy. The dependence of $\sigma_{F\theta\alpha}$ on s and t is shown in Fig. 8.

Stage (III). Propagation of cleavage crack across ferrite grain boundary

We assume fracture condition of propagation of a cleavage crack across ferrite grain boundary as

$$\sigma_n \geq \sigma_{F\alpha\alpha} \quad (9)$$

where σ_n can be calculated by the equation same as that for Stage (II), i.e. Eq. (6). On the other

hand, $\sigma_{F\alpha\alpha}$ is local fracture stress for Stage (III) formulated based on the Griffith theory, as

$$\sigma_{F\alpha\alpha} = \sqrt{\frac{\pi E \gamma_{\alpha\alpha}}{(1-\nu^2)D}} \tag{9}$$

where D is a diameter of cleaved surface formed in Stage (II) and $\gamma_{\alpha\alpha}$ is an effective surface energy for a cleavage crack in a ferrite grain to propagate across grain boundary. It is assumed that $\gamma_{\alpha\alpha}$ depends on temperature because plastic deformation below cleavage fracture surface changes with temperature [10]. Temperature dependence of $\gamma_{\alpha\alpha}$ is thus assumed based on the experimental results by San Martin and Rodriguez-Ibabe [11], as shown in Fig. 9. Although the figure shows steep increase at temperature higher than -70°C, the present study employs the value of $\gamma_{\alpha\alpha}$ in the temperature range lower than -80°C.

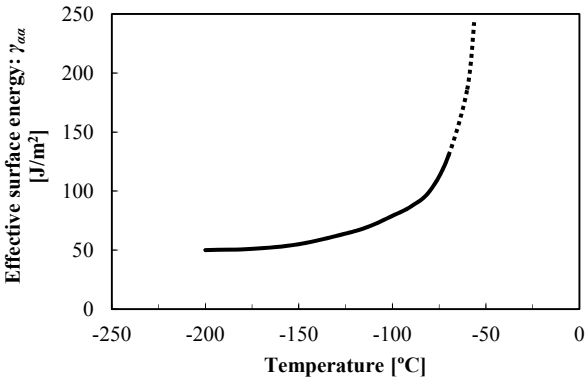

Fig. 9 Effective surface energy for across grain boundary [11]

3. Development of Numerical Model

Considering the fracture conditions of the three stages described in the previous section, a numerical model of the cleavage fracture initiation of ferrite-cementite steels is developed. Procedures of the modeling are described as follows.

(a) A domain where the cleavage fracture initiation is possible to occur is defined as an active zone.
(b) The active zone is divided by cubic volume elements of the same size. It is noted that the size of the volume elements must be larger than the maximum grain size. A schematic view of the volume element is shown in Fig. 10.
(c) Ferrite grains are assigned at random in each volume element based on ferrite grain size distribution until sum of the volume of the assigned grains reaches that of the elemental volume. At the same time, crystallographic orientation of each grain is determined at random.
(d) Cementite particles are assigned in each volume element based on cementite particle thickness (minor axis) distribution. The shape of the cementite is approximated as a prolate spheroid.
(e) Macroscopic elasto-plastic FEA is performed based on true stress-strain curve and stress tensor and a maximum principal plastic strain at each volume element are evaluated at each step time. In the calculation, step time increments are defined for the evaluation of the cleavage fracture initiation at the same time.
(f) The cleavage fracture initiation process based on the three stages is evaluated in each volume element for a time step as following (g) ~ (k).
(g) For Stage (I), cracked cementite particle distribution is evaluated based on Eq. (4) by using the distribution of cementite particle thickness in the volume element.
(h) For the stage (II), first, two ferrite grains (Grain A and Grain B) adjacent to the respective cracked cementite obtained in [g] are selected at random. Grain A and Grain B are used for the evaluation of σ_n in Eq. (6) and $\sigma_{F\theta\alpha}$ in Eq. (7), respectively. Assuming the location of the each cementite particle on the boundary of Grain B, the length of dislocation line s is determined. Then, the evaluation of fracture condition of Stage (II) is carried out based on Eq. (5) for all the combinations of the ferrite grains and the cracked cementite particles. If the fracture condition is satisfied, a cleavage crack is assumed to form in Grain A and the cleaved

grain is excluded in following time steps.

(i) In the case that Stage (II) is satisfied, Stage (III) is then evaluated. First, an additional grain (Grain C) is selected at random. Then, $\sigma_{F\alpha\alpha}$ and σ_n in Eq. (8) are respectively calculated by using Grain A and of Grain C, and the fracture condition of Stage (III) is evaluated.

(j) Cleavage fracture is assumed to be initiated at the time when the fracture condition of Stage (III) is satisfied in any one of the volume elements. That is a "weakest link" assumption in this model.

(k) If the fracture is not initiated, the calculations of (f) ~ (j) are carried out for the next time step.

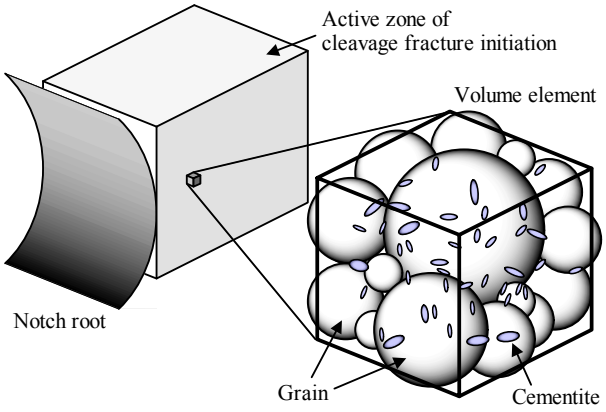

Fig. 10 Modeling of volume element

4. Simulation of Fracture Toughness Testing

4.1 Experiment

Three point bending test using notched specimens was conducted. The specimen was machined from the steels 10LL, 10LS, 5SL and 5SS, which were used in Section 2.2. Configuration of the specimen is shown in Fig. 11. Test temperature was changed between -150°C and -80°C. Loading rate was 1 mm/min. Notch opening displacement was measured by a clip gauge attached to the edge of the notch.

Quasi-CTOD is introduced as a parameter to evaluate the fracture toughness. The quasi-CTOD is calculated by simply applying the CTOD estimation formula [12], as

$$\delta = \frac{K^2(1-\nu^2)}{2\sigma_Y E} + \frac{r_p(W-a)V_p}{r_p(W-a)+a+z} \tag{9}$$

where K is a stress intensity factor, σ_Y is a yield stress at a test temperature, r_p is the rotation factor (= 0.4), W is the width of the specimen (= 20 mm), a is the notch depth (= 7 mm), z is the distance of the notch opening gauge location above the specimen surface (= 0 mm), V_p is plastic component of the notch opening displacement. It is noted that the quasi-CTOD does not represent physical crack tip opening displacement but just represents intensity of deformation at the notch root. Critical values of the quasi-CTOD are used for a validation of the developed model.

4.2 Model conditions

In the procedure (a), the active zone is defined as a rectangular parallelepiped whose side lengths are 1.6 mm, 1 mm and 20.0 mm in respective directions of the width, the axis and the thickness of the specimen, based on the preliminary observation of the fracture initiation points.

The size of each volume element in the procedure (b) is also defined as a rectangular parallelepiped. The side lengths are 0.2 mm, 0.167 mm and 0.2 mm in the respective directions. This is nearly equivalent to the size of a sphere whose diameter is 0.25 mm. The number of the volume elements is 6,000 in the active zone as a result.

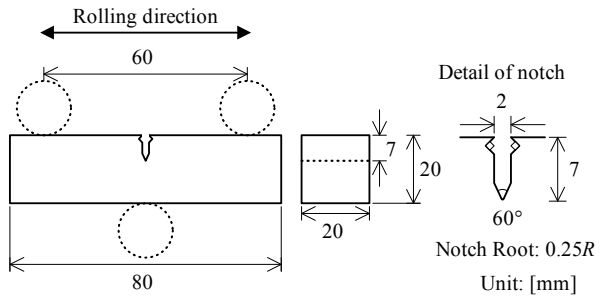

Fig. 11 Configuration of three point-bend specimen

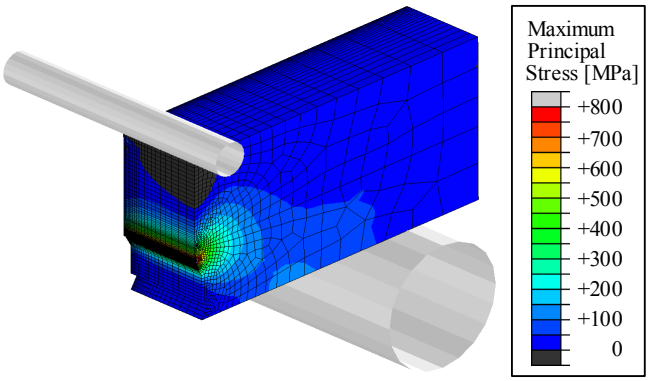

Fig. 14 Mesh division and stress distribution in FEA (10LL, -120°C)

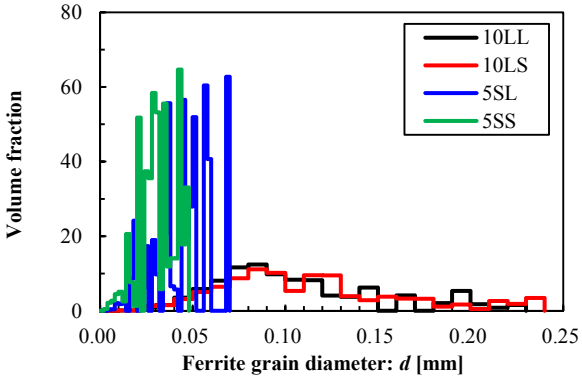

(a) Ferrite grain diameter

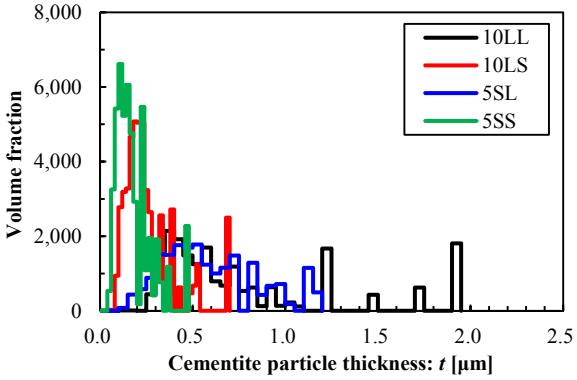

(b) Cementite particle thickness

Fig. 13 Distributions of ferrite grain diameter and cementite particle thickness

In the procedures (c) and (d), The ferrite grains and the cementite particles are assigned at random in each volume element based on their distributions shown in Fig. 13.

A quarter-symmetry finite element model is used to obtain stress and strain distributions in the active zone in the procedure (e). Displacement is applied by the jig. The mesh division and an example of the calculated stress distribution are shown in Fig. 14.

4.3 Results and discussions

Comparisons of the experimental results and the prediction values of the critical quasi-CTOD are shown in Fig. 15. The predicted values show good agreements with the experimental results in all the steels. The variation of the predicted critical values under the same conditions is derived from the stochastic nature of the developed model, i.e., the toughness scatter is derived from the statistical size distributions of ferrite grains and cementite particles. It is obviously found that the transition curve of the critical quasi-CTOD is shifted to lower temperature for finer ferrite grain steel. In addition, the same tendency is found for smaller cementite particle steel.

In the results of the respective steels, the predicted values reproduce the tendency that lower temperature makes lower values of the critical quasi-CTOD. The predicted values at high temperature are evaluated with high accuracy. On the other hand, the results at low temperature are underestimated in some cases. As causes of this result, an excessive cementite cracking in Stage (I) and accuracies of the effective surface energies $\gamma_{\theta\alpha}$ in Stage (II) and $\gamma_{\alpha\alpha}$ in Stage (III) might be

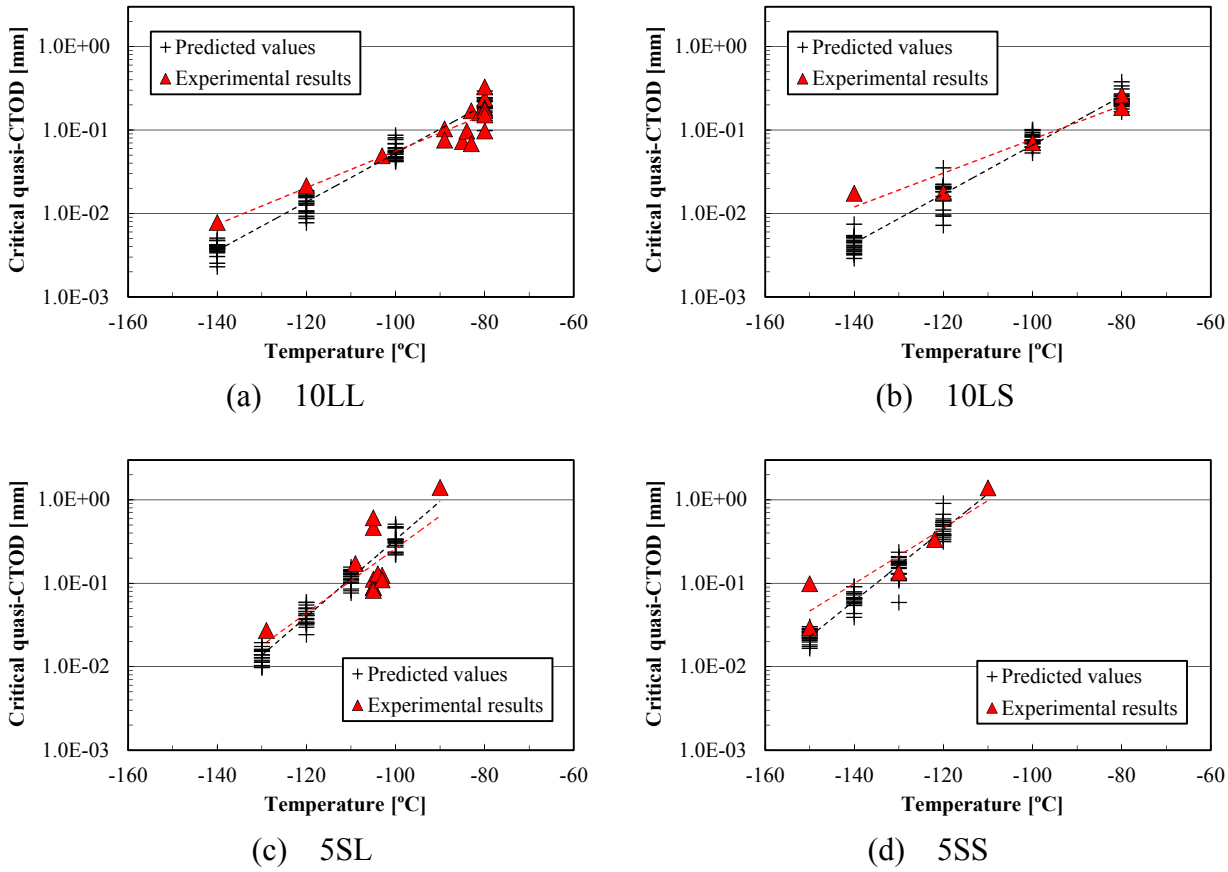

Fig. 15 Comparison between experimental and numerical results of critical quasi-CTOD

pointed out. In order to improve this problem, modification of the formulation of the ratio of the cementite cracking considering the shape of the cementite particles, and quantitative and accurate estimations of $\gamma_{\theta\alpha}$ and $\gamma_{\alpha\alpha}$ must be required. The maximum differences of the transition temperatures between the experimental results and the predicted values is however 15°C. Based on the aforementioned results, the validation and the effectiveness of the proposed model are found out.

5. Conclusions

A numerical model to quantitatively evaluate a cleavage fracture initiation in ferrite-cementite steel was developed. The model is based on the microscopic fracture process of the three stages; (I) formation of fracture origin by cementite cracking, (II) propagation of the cementite crack into ferrite matrix and formation of a cleavage crack, and (III) propagation of cleavage crack across ferrite grain boundary.

The fracture conditions of respective stages were formulated. The fracture condition of Stage (I) is formulated as a ratio of cementite cracking based on experimental results of a tensile testing with notched specimens and SEM observation using steels with various ferrite and cementite sizes. The fracture conditions of Stage (II) and Stage (III) were formulated based on the concept of the fracture stress.

In the development of numerical model, an active zone is defined and divided into volume elements. Ferrite grains and cementite particles are assigned based on their distributions into each volume

element. Strain and stress at each volume element are evaluated by macroscopic FEA. Cleavage fracture is assumed to initiate at the time when the fracture conditions of the all stages are satisfied in any one of the volume element.

The developed model was validated by three point bend testing of notched specimens using steels with various ferrite and cementite sizes. The numerical predicted values of fracture toughness show good agreement with the experimental results for all cases. It is therefore concluded that the proposed model is effective to predict the fracture toughness of ferrite-cementite steels.

Acknowledgements

Part of the present work was funded by the Fundamental Research Developing Association Shipbuilding Offshore. The authors would like to thank the members of the forum of the Iron and Steel Institute of Japan for their valuable discussions.

References

[1] W.C. Leslie, The Physical Metallurgy of Steels, Mcgraw-Hill College, 1981.
[2] D.A. Curry, J.F. Knott, Effects of microstructure on cleavage fracture stress in steel. Metal Science, 12 (1978) 511-514.
[3] E.A. Almond, D.H. Timbres, J.D. Embury, The influence of second phase particles on fracture. Proceedings of the International Conference on Fracture, 2 (1969) 253-265.
[4] N.J. Petch, The influence of grain boundary carbide and grain size on the cleavage strength and impact transition temperature of steel. Acta Metallurgica, 34 (1986) 1387-1393.
[5] M.S. Bingley, Effect of grain size and carbide thickness on impact transition temperature of low carbon structural steels. Materials Science and Technology, 17 (2001) 700-714.
[6] F.M. Beremin, A local criterion for cleavage fracture of a nuclear pressure vessel steel. Metallurgical and Materials Transactions A, 14 (1983) 2277-2287.
[7] OIM Data Collection User's Manual, TexSEM Laboratories, 2007.
[8] W.S. Rasband, ImageJ, U. S. National Institutes of Health, Bethesda, Maryland, 2011, http://rsb.info.nih.gov/ij/.
[9] A.S. Tetelman, A.J. McEvily, Jr. Fracture of Structural Materials, John Wiley & Sons, Inc., New York, 1967.
[10] Tsann Lin, A.G. Evans, R.O. Ritchie, Stochastic modeling of the independent roles of particle size and grain size in transgranular cleavage fracture. Metallurgical and Materials Transactions A, 18 (1987) 641-651.
[11] J.I. San Martin, J.M. Rodriguez-Ibabe, Determination of energetic parameters controlling cleavage fracture in a Ti-V microalloyed ferrite-pearlite steel. Scripta Materialia, 40 (1999) 459-464.
[12] BS 7448: Part 1, Fracture Mechanics Toughness Tests, Part 1, Method for Determination of K_{Ic}, Critical CTOD and Critical J Values of Metallic Materials, British Standard Institution, 1991.